Angewandte Chemie International Edition

Angewandte International Edition Chemie

How to cite: *Angew. Chem. Int. Ed.* **2026**, e1788393
doi.org/10.1002/anie.1788393

RESEARCH ARTICLE OPEN ACCESS

Isolation and Reactivity of a Square-Planar Trisamido Silane

David M. J. Krengel[1] | Xiaobai Wang[1] | Christopher Golz[2] | Regine Herbst-Irmer[1] | Oliver P. E. Townrow[3] | Malte Fischer[1]

[1]Institut Für Anorganische Chemie, Georg-August-Universität Göttingen, Tammannstraße 4, Göttingen, Germany | [2]Institut Für Organische und Biomolekulare Chemie, Georg-August-Universität Göttingen, Tammannstraße 2, Göttingen, Germany | [3]Institute of Nanotechnology, Karlsruher Institut für Technologie, Hermann-von-Helmholtz-Platz 1, Eggenstein-Leopoldshafen, Germany

Correspondence: Oliver P. E. Townrow (oliver.townrow@kit.edu) | Malte Fischer (malte.fischer@uni-goettingen.de)

Received: 15 December 2025 | **Revised:** 6 March 2026 | **Accepted:** 26 March 2026

Keywords: aromaticity–rearomaticity switch | element–ligand cooperativity | main-group chemistry | silicon | structural constraint

ABSTRACT

Square-planar coordination at tetravalent silicon is highly disfavored, rendering structurally authenticated Si(+IV) complexes of this type exceedingly rare. Herein, we report the synthesis and isolation of a square-planar silicon(+IV) hydride supported by an unsymmetric, trianionic *N*,*N*,*N*-pincer ligand with a dearomatised backbone. Single-crystal X-ray diffraction confirms a strictly planar, four-coordinate silicon centre, with spectroscopic data and quantum-chemical calculations providing complementary support for this bonding motif. Reactivity studies demonstrate element–ligand cooperative substrate activation driven by ligand rearomatisation, thereby paralleling constant-oxidation-state transformations in late transition metal systems and challenging the prevailing reliance on low-valent p-block species for bond activation.

1 | Introduction

Silicon, the second most abundant element in Earth's crust, occurs nearly exclusively as tetrahedral Si(+IV) in silicates and related materials [1]. While this oxidation state defines the conventional chemistry of silicon, the discovery of low-valent species, ranging from silylenes [2–6] to heavier silicon-based alkene and alkyne analogues [7–9], silylium ylidenes [10–13] and silylones [14–16], has unveiled striking reactivity patterns and inspired catalytic applications [17–20]. Consequently, modern molecular silicon chemistry has almost been entirely devoted to low oxidation state species, whereas Si(+IV) has remained confined to its classical role as a fully oxidized precursor.

Beyond oxidation state, however, the reactivity of an element is profoundly influenced by the nature and topology of its coordination environment and the concept of structural / geometric constraint has recently emerged as a powerful design element in main-group chemistry, altering the behaviour of main-group elements [21–24]. While this strategy has flourished in Group 13 [25–31] and especially Group 15 [32–45] chemistry in recent years, it remains far less explored for Group 14 elements [46–54].

For silicon, deviations from the canonical tetrahedral geometry have long been predicted and, in isolated cases, observed. Planar-tetracoordinate silicon (ptSi) motifs in lower oxidation states have been detected in the gas phase (**I**) [55], embedded in polysilanes (e.g. **II**) [56, 57], or ligated by transition metals (**III**; Scheme 1, A) [58]. Only in 2021 did Greb and co-workers isolate a square-planar Si(+IV) compound (**IV**), an intrinsically stable crystalline species that challenges traditional boundaries of silicon chemistry (Scheme 1, A) [59]. The compound employs a highly symmetric calix[4]pyrrolato ligand, which has proven exceptionally effective in stabilising and exploiting structurally and geometrically constrained p-block complexes [23]. The same group recently employed another highly symmetric, macrocyclic

In memory of Prof. Herbert W. Roesky

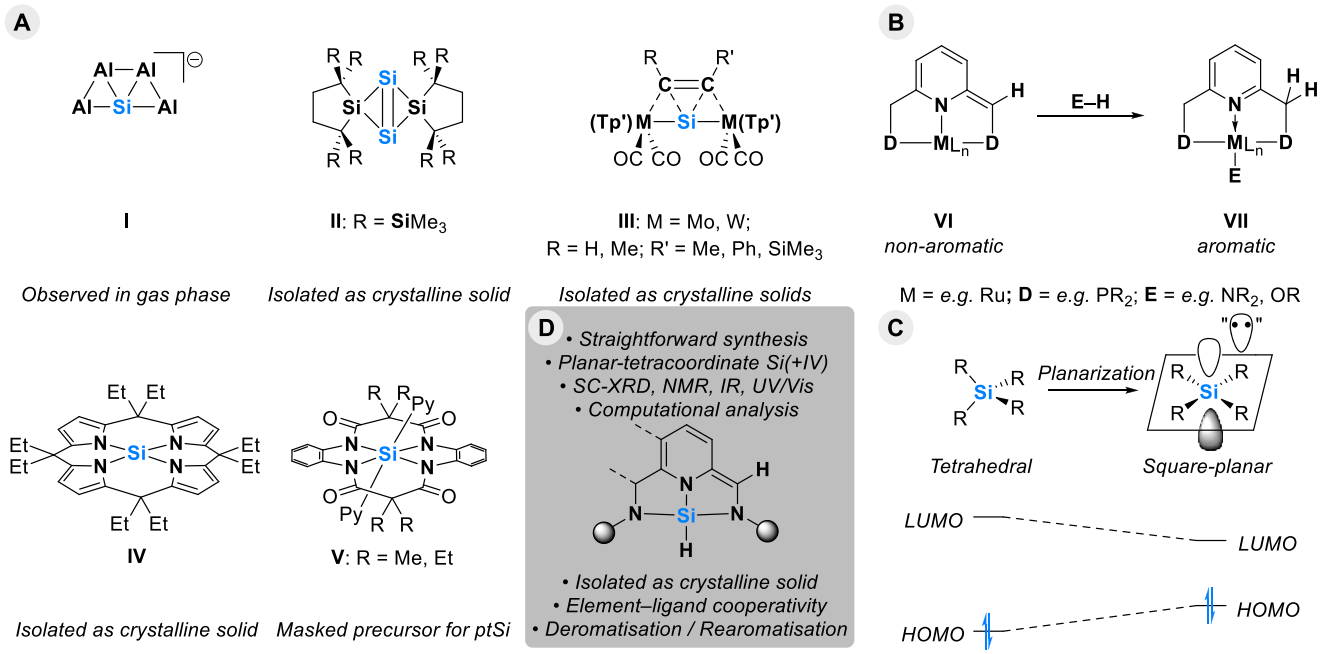

SCHEME 1 | (A): Reported compounds **I**-**III** with planar-tetracoordinated silicon in lower oxidation states as well as the first ptSi(+IV) compound **IV** and the masked ptSi(+IV) complex **V** [Tp' = k^3-*N*,*N*,*N*-hydridotris(3,5-dimethylpyrazolyl)borate]; (B): Element–ligand cooperativity in constant oxidation state transition metal catalysis; (C): Planarisation from tetrahedral Si(+IV) to square-planar geometry and its impact on the frontier molecular orbital energies of HOMO and LUMO; (D): This work.

and tetra-amido-based ligand to isolate the bis(pyridine) Si(+IV) adduct **V**, which can be regarded as a masked source of ptSi(+IV) and is found to catalyse the 1,4-hydroboration of pyridines (Scheme 1, A) [54].

In theory, the square-planar geometry of Si(+IV) represents a high-energy transition state along the inversion pathway [60–62], yet the isolated ptSi(+IV) complex **IV** exhibits unique photochemical and cooperative reactivity reminiscent of transition-metal systems [59].

Ligand-to-element charge transfer and element–ligand cooperativity (ELC) are central to this behaviour, echoing Milstein's seminal transition-metal related paradigm of ligand-assisted bond activation and catalysis without a formal change in oxidation state (**VI** and **VII** in Scheme 1, B) [63–65]. Within this framework, the ability of the supporting ligand to switch between aromatic and non-aromatic states serves as a powerful driving force for these challenging transformations.

This cooperative concept has also emerged recently as a tool in other areas of the main-group where redox-cycling is unfavourable, allowing precious metal chemistry such as hydrogenation catalysis with magnesium and calcium complexes [66–68]. Harnessing ELC at Si(+IV) centres could bridge transition-metal and main-group reactivity, opening the door to redox-neutral, metal-free bond activation and catalysis based on this sustainable element.

Computational analyses reveal that formal planarisation of a tetrahedral Si(+IV) centre to a square-planar geometry markedly lowers the energy of the lowest unoccupied molecular orbital (LUMO), a silicon-centred p_z-type orbital. Concurrently, the predominantly ligand-centred highest occupied molecular orbital (HOMO) is raised in energy, resulting in a narrowed HOMO–LUMO energy gap, an electronic signature reminiscent of low-valent p-block and d-block species (Scheme 1, C) [62, 69, 70]. These features underscore the unique potential of ptSi(+IV) compounds for redox-neutral bond activation and other applications in catalysis, photochemistry, and materials science [71–76].

Here, we report a square-planar Si(+IV) compound, a crystalline tris(amino)silane of the type (NNN)Si(H) that combines an unsymmetric pincer-type scaffold with the distinct electronic structure of ptSi(+IV), establishing a robust platform for exploring element–ligand cooperativity in silicon chemistry (Scheme 1, D). As a proof-of-principle demonstration, we present its ability to activate an alkyne *via* rearomatisation of its ligand backbone.

2 | Results and Discussion

Our investigation began with the preparation of the tridentate quinoline-based ligand precursor **L1**, which bears a secondary amine functionality and an imine side arm, following a slightly modified literature procedure (Scheme 2) [76]. Notably, Hwang and co-workers recently employed this ligand to promote O_2 activation using geometrically constrained Group 15 compounds [77]. **L1** was obtained as a yellow crystalline solid, and its structure was confirmed by single-crystal X-ray diffraction (SC-XRD; Figure S66), unequivocally confirming the *E*-configuration of the imine double bond. In addition, ^{15}N NMR spectroscopic measurements were performed to facilitate future comparisons (vide infra) [78].

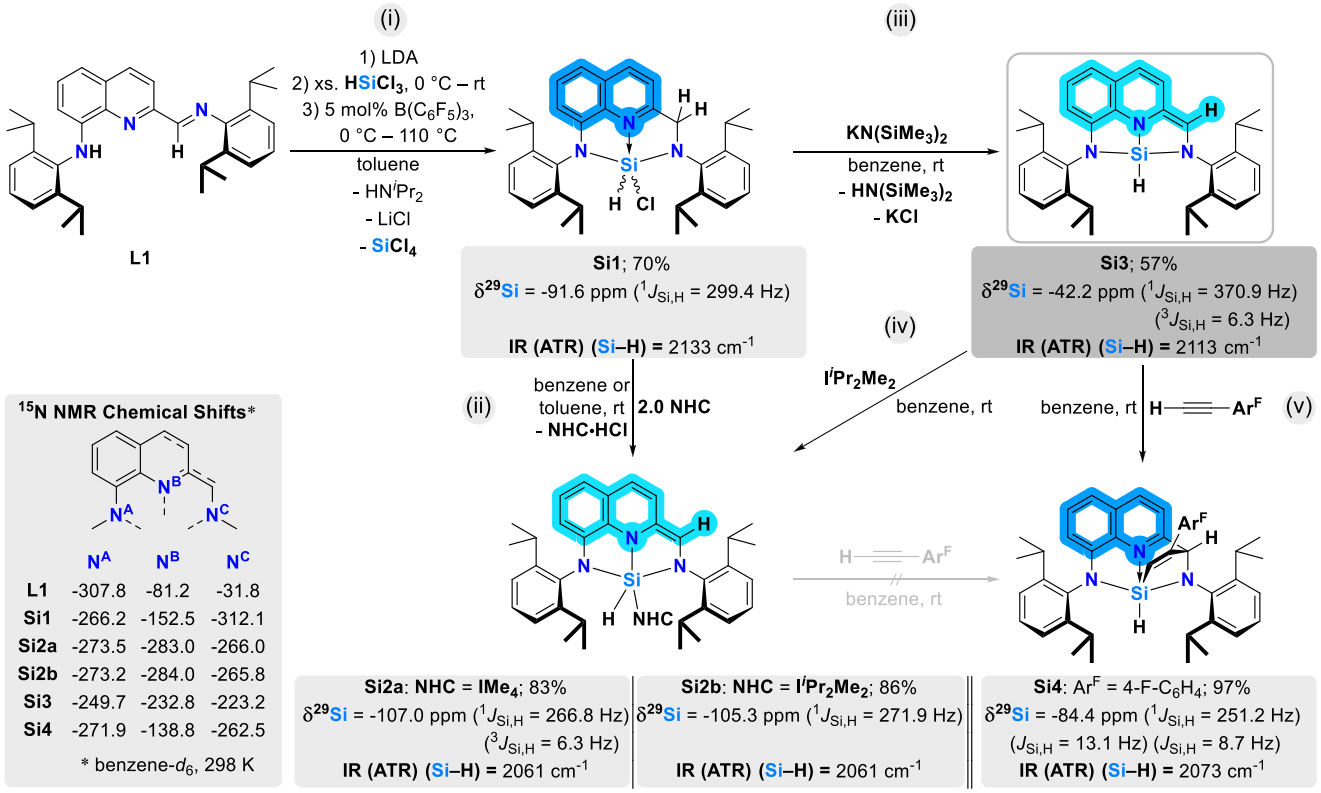

SCHEME 2 | Preparation and selected analytical data of the reported compounds. (i) Synthesis of **Si1** from ligand precursor **L1** *via* a one-pot deprotonation with lithium diisopropylamide (LDA), trichlorosilane ($HSiCl_3$) addition and Lewis-acid assisted (use of tris(pentafluorophenylborane) reaction sequence. (ii) Reaction of **Si1** with two equivalents of selected *N*-heterocyclic carbenes (NHCs) to yield the NHC-stabilised silanes **Si2a**,**b**. (iii) Synthesis of the square-planar silane **Si3** *via* dehydrohalogenation with potassium hexamethyldisilazide ($KN(SiMe_3)_2$). (iv) Alternative preparation of **Si2b** *via* NHC addition to **Si3**. (v) Element–ligand cooperative activation of 1-fluoro-4-ethynylbenzene with **Si3** to yield the activation product **Si4**.

With **L1** in hand, a one-pot protocol for the synthesis of the corresponding chlorosilane **Si1** was developed. Deprotonation with lithium diisopropylamide (LDA), followed by the addition of an excess of trichlorosilane ($HSiCl_3$), with the latter reagent simultaneously reducing the imine side arm to the corresponding aminosilane and introducing the 'HSiCl' moiety into the *N*,*N*,*N* pocket of the in situ generated dianionic ligand environment [79]. This transformation was only successful in the presence of catalytic amounts (5 mol%) of tris(pentafluorophenyl)borane ($B(C_6F_5)_3$) as a Lewis acid additive [78]. After work-up, **Si1** was isolated as an orange solid in 70% yield (Scheme 2).

Si1 was comprehensively characterized by multinuclear NMR, infrared (IR), UV/Vis spectroscopy and liquid injection field desorption ionization (LIFDI) mass spectrometry [78]. Particularly diagnostic information was obtained from multinuclear and 2D NMR spectroscopy. In solution, **Si1** shows hindered rotation of the flanking aryl groups on the NMR time scale, as evidenced by the detection of one doublet and one heptet signal in the ^{1}H NMR spectrum for each of the methyl and methine hydrogen atoms of the diisopropylphenyl (Dipp = 2,6-^{i}Pr$_2$-C$_6$H$_3$) substituents, respectively. The diastereotopic methylene group gives rise to two characteristic doublet signals at δ^1H = 4.05 and 4.42 ppm, each with a diagnostic $^2J_{H,H}$ coupling constant of 20.0 Hz. The ^{29}Si resonance appears at δ^{29}Si = −91.6 ppm with a $^1J_{Si,H}$ coupling constant of 299.4 Hz. This chemical shift is consistent with other chlorosilanes such as [{PhC(N^{t}Bu)$_2$}Si(H)Cl$_2$] [80] (δ^{29}Si = −96.8 ppm) or [{^{Dipp}NC(H)═C(H)–C(H)═N^{Dipp}}Si(H)Cl$_2$] (δ^{29}Si = −97.4 ppm) [81], supporting the assignment of a five-coordinate silicon centre in **Si1**. The corresponding ^{1}H NMR resonance of the Si–H moiety is observed as a sharp singlet at δ^1H = 5.89 ppm, shifted upfield relative to [{PhC(N^{t}Bu)$_2$}Si(H)Cl$_2$] (δ^1H = 6.70 ppm) [80] and [{^{Dipp}NC(H) = C(H)–C(H) = N^{Dipp}}Si(H)Cl$_2$] (δ^1H = 6.46 ppm) [81], and intermediate between values reported for the diamino(chloro)silanes [{N^{t}BuCH}$_2$Si(H)Cl] (δ^1H(SiH) = 6.35 ppm; (δ^{29}Si = −38.4 ppm) [82] and [{(N(SiMe$_3$)$_2$)$_2$-ferrocene-1,1'-diyl}Si(H)Cl] ((δ^1H(SiH) = 5.72 ppm; δ^{29}Si = −31.8 ppm) [83] with four-coordinate silicon centres. In the solid-state IR spectrum of compound **Si1**, the characteristic Si–H stretching band, typically observed between 2100 and 2250 cm^{-1} [84], appears at 2133 cm^{-1}. It is worth mentioning that although crystals could be obtained through multiple crystallisation strategies, they invariably afforded diffraction data of insufficient quality for rigorous structural refinement; nonetheless the connectivity of the molecular framework could principally be confirmed.

Subsequent attempts to generate the corresponding silane with a reduced quinoline backbone focused on dehydrohalogenation of the chloride ligand bound to silicon and the adjacent methylene unit of the backbone. Treatment of **Si1** with the *N*-heterocyclic carbene (NHC) I^{i}Pr$_2$Me$_2$ (I^{i}Pr$_2$Me$_2$ = 1,3-diisopropyl-4,5-dimethylimidazol-2-ylidene) resulted in an unprecedented and highly selective manner, in a 1:2 stoichiometric transformation, affording I^{i}Pr$_2$Me$_2$•HCl as byproduct

and the NHC-stabilised silane **Si2b** with the targeted reduced quinoline backbone and NHC-ligation (Scheme 2) [85]. Notably, the reaction of chlorosilanes with NHCs is an established route to silylenes *via* dehydrohalogenation at the silicon centre, driven by imidazolium-salt formation [86, 87]. In the present case, however, it is the protic exocyclic hydrogen atom that is removed, rather than the predominantly hydridic silicon-bound hydrogen atom.

Si2b was isolated as a red solid in 86% yield. LIFDI-MS analysis supported its formation *via* clean detection of the M^+ signal (Figure S32). Definitive evidence for reduction of the quinoline backbone arises from the disappearance of the CH_2 group in both the ^1H and $^{13}C\{^1H\}$ NMR spectra, along with the appearance of the remaining hydrogen atom at the former imine α-position. This proton resonates at $\delta^1H = 6.08$ ppm as a doublet ($^4J_{H,H} = 1.5$ Hz), coupling to the Si–H hydrogen atom, as confirmed by $^1H/^1H$ COSY NMR spectroscopy. The Si–H signal appears as a multiplet at $\delta^1H = 7.12$ ppm, significantly downfield relative to the starting material **Si1**. The multiplet pattern results from the aforementioned coupling as well as through-space interaction with one of the methine hydrogen atoms of the isopropyl substituents on the coordinated NHC, the latter giving rise to a diagnostic doublet of heptet signal. The ^{29}Si NMR resonance of **Si2b** is only slightly shifted compared to **Si1**, appearing at $\delta^{29}Si = -105.3$ ppm as a doublet ($^1J_{Si,H} = 271.9$ Hz), consistent with retention of five-coordinate silicon and preservation of the +IV oxidation state. Likewise, the Si–H stretching band is shifted to lower wavenumbers (2061 cm^{-1}). The $^{13}C\{^1H\}$ resonance of the carbene carbon is observed at $\delta^{13}C\{^1H\} = 154.2$ ppm, essentially identical to that reported for the NHC-stabilised dichlorosilane [{IMe_4}$Si(Cl_2)H_2$] ($\delta^{13}C\{^1H\} = 154.1$ ppm; IMe_4 = 1,3,4,5-tetramethylimidazol-2-ylidene) [88]. Notably, $^1H/^{15}N$ HMBC NMR spectroscopy allows assignment of all nitrogen atoms in both **Si1** (three) and **Si2b** (five) to their respective resonances, revealing characteristic changes in the ^{15}N NMR chemical shifts of the quinoline moiety: in **Si1**, $\delta^{15}N = -312.1$ ($N_{Aryl,Alkyl}$), -266.7 (N_{Aryl2}), -152.5 (N_{Quin}) ppm, whereas in **Si2b**, $\delta^{15}N = -284.0$ (N_{Quin}), -273.2 (N_{Aryl2}), -265.8 ($N_{Aryl,NCH}$), -191.4 (N_{NHC}), -183.4 (N_{NHC}) ppm (Scheme 2). These observations provide unambiguous proof of the non-aromatic nature of the quinoline backbone in **Si2b**.

Additionally, crystals of **Si2b** suitable for SC-XRD were obtained from a saturated toluene solution at −30°C and the molecular structure is shown in Figure 1.

Si2b crystallises in the monoclinic space group $P2_1/n$ with four molecules per unit cell. The five-coordinate silicon centre adopts a distorted square-pyramidal coordination environment, as indicated by the τ_5 geometry index of $\tau_5 = 0.31$. It is bound to a freely refined hydrogen atom, the three nitrogen donors of the pincer-ligand scaffold and the NHC carbon atom [89]. The Si1—C35 bond length of 1.967(2) Å falls within the range reported for structurally authenticated, NHC-stabilised five-coordinate silicon centres in the +IV oxidation state [85]. All three silicon-bound nitrogen atoms are planarised, as reflected in the sums of valence angles around these atoms (N1: 360.0°, N2: 356.8°, N3: 358.8°) and their Si—N bond lengths agree with the single-bond covalent radii of silicon and nitrogen ($\Sigma_{cov,r}$(Si–N) = 1.87 Å [90, 91]). Notably, the Si1–N1 distance is significantly shortened (1.7528(18) Å). Within the quinolide heterocycle, the C—C bond lengths across the C_6H_4 ring support substantial π-delocalisation, whereas the C1—C2 (1.426(3) Å), C2—C3 (1.359(3) Å) and C3—C4 (1.456(3) Å) distances in the C_5NH_2 moiety are more differentiated and consistent with a localised carbon–carbon double bond between C2 and C3 ($\Sigma_{cov,r}$(C=C) = 1.34 Å [90, 91]). The exocyclic C1—C10 bond lengths of 1.362(3) Å, also characteristic of a respective double bond, further supports the non-aromatic nature of the ligand.

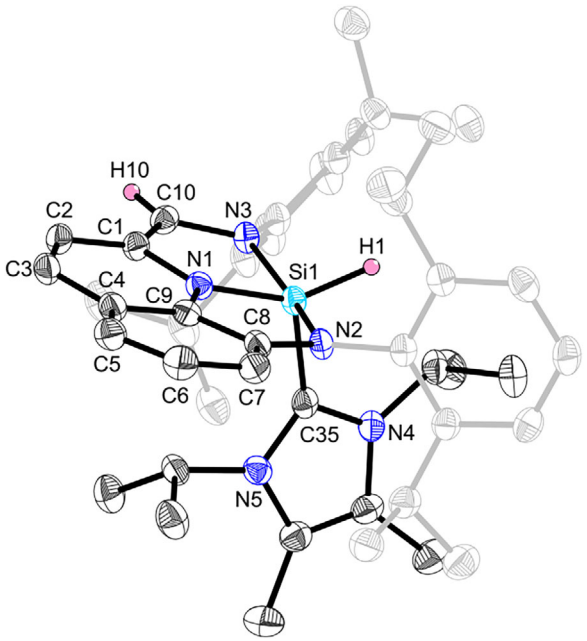

FIGURE 1 | Molecular structure of **Si2b** in the crystal. Anisotropic displacement parameters are drawn at the 50% probability level (hydrogen atoms, except for H1 and H10, and disorder have been omitted for clarity). Selected bond lengths (Å) and angles (deg): Si1–C35 1.967(2), Si1–N1 1.7528(18), Si1–N2 1.9001(18), Si1–N3 1.8763(18), N2–C8 1.395(3), C7–C8 1.397(3), C8–C9 1.394(3), C6–C7 1.402(3), C5–C6 1.389(3), C4–C5 1.406(3), C4–C9 1.391(3), C3–C4 1.456(3), C2–C3 1.359(3), C1–C2 1.426(3), N1–C1 1.414(3), N1–C9 1.382(3), C1–C10 1.362(3), N3–C10 1.395(3), N2–Si1–N3 162.46(8), N1–Si1–N2 82.77(8), N1–Si1–N3 82.34(8), N1–Si1–C35 115.06(9), N2–Si1–C35 96.21(8), N3–Si1–C35 98.47(8).

To further demonstrate the scope of this NHC-induced transformation, the reaction of **Si1** with IMe_4 afforded a second derivative, **Si2a**. As its spectroscopic features are essentially identical to those of **Si2b**, a detailed discussion is omitted at this point [78].

Given this transformation, we next asked ourselves whether a non-base-stabilised analogue of **Si2a**,**b** could be accessed synthetically by direct reaction with an appropriate dehydrohalogenation reagent. To our delight, treatment of **Si1** with potassium hexamethyldisilazide ($KN(SiMe_3)_2$) in a 1:1 ratio effected a clean transformation accompanied by salt formation of KCl and formation of $HN(SiMe_3)_2$ as by-product. This procedure afforded a singly silicon-containing product, **Si3**, which was isolated in 57% yield as a yellow solid (Scheme 2). Slow evaporation of a THF/*n*-hexane solution of **Si3** furnished single crystals suitable for SC-XRD analysis but the crystals exhibit intrinsic disorder throughout the molecule. In contrast, slow evaporation of a saturated diethyl ether solution at -30°C yielded a second polymorph distinct from that obtained from THF/*n*-hexane and other solvent

combinations. Subsequent crystallographic analysis revealed one and a half crystallographically independent molecules in the asymmetric unit in which one displays disorder about a two-fold axis, whereas the second is fully ordered. The molecular structure of the ordered molecule is shown in Scheme 3, A, and only its structural parameters are discussed herein. The structural analysis unambiguously confirms a four-coordinate silicon centre. The hydride ligand was located in the difference Fourier map and freely refined. The coordination geometry at silicon is square planar, as supported by the τ_4 and $\tau_{4'}$ geometry indices of 0.10 and 0.07, respectively [92, 93]. Accordingly, **Si3** represents only the second molecular, crystalline Si(IV) species reported to adopt a square-planar geometry. This finding demonstrates that tetravalent silicon can access such a coordination environment even in the absence of a highly symmetric tetraanionic four-donor ligand framework, and notably when one of the ligands is merely a hydride. The Si—N bond lengths (Si1–N1 1.797(4) Å, Si1–N2 1.747(5) Å and Si1–N3 1.784(4) Å; $\Sigma_{cov,r}$(Si–N) = 1.87 Å [90, 91]) fall within a narrow range ($\Delta < 0.05$ Å), indicative of nearly equivalent nitrogen donor interactions within the trisamido trianionic ligand scaffold. Consistent with this interpretation, all three nitrogen atoms adopt trigonal planar coordination environments, supporting their assignment as sp^2-hybridised amido donors. Structural analysis of the C_5NH_2 backbone is in good agreement with that of the NHC-stabilised congener **Si2b**, further corroborating the electronic description of the ligand framework. The C19–C20 (1.349(8) Å) and exocyclic C21–C22 (1.363(8) Å) bond lengths are clearly consistent with localised C═C double bonds, whereas the adjacent C15–C19 (1.456(8) Å) and C20–C21 (1.443(8) Å) distances are significantly elongated and characteristic of single bonds. This pronounced bond length alternation unambiguously demonstrates that the π-electron density is not uniformly delocalised across the ligand backbone, thereby supporting a non-aromatic description of this moiety.

Further clear evidence for the non-aromatic nature of the ligand derives from the ^{15}N NMR data: the three nitrogen resonances of the pincer scaffold differ by only a maximum of $\Delta\delta^{15}$N = 26.5 ppm (Scheme 2), reflecting the nearly identical SC-XRD bond metrics at all three nitrogen atoms, aligning well with **Si2b**, which also features the dearomatised backbone. Since dimerisation has been observed for structurally similar silicon(+IV) complexes supported by tridentate *N,N,N* ligands in solution [94], external calibration curve diffusion-ordered ^{1}H NMR spectroscopy (ECC-^{1}H-DOSY) with adamantane as internal standard was employed to establish the aggregation state of **Si3** in solution. The diffusion coefficient obtained from ECC-^{1}H-DOSY analysis unambiguously confirms that **Si3** is monomeric in solution (Figure S44; Table S1) [95, 96]. The ^{29}Si NMR spectrum of **Si3** exhibits a diagnostic doublet-of-doublets resonance at δ^{29}Si = −42.2 ppm. When compared to the five-coordinate silicon precursor **Si1** (δ^{29}Si = −91.6 ppm) and five-coordinate base-stabilised analogue **Si2b** (δ^{29}Si = −105.3 ppm), the pronounced downfield shift is characteristic of a tetracoordinate silicon atom and is also shifted to lower field relative to **IV** (δ^{29}Si = -55.6 ppm) [59]. The corresponding $^1J_{Si,H}$ coupling constant of 370.9 Hz is at least 71 Hz larger than those observed for the five-coordinate silanes discussed above and ranks among the highest $^1J_{Si,H}$ coupling constants reported for four-coordinate silicon species [97]. Furthermore, it is significantly larger than that observed for a trisamido silane featuring a tetrahedral silicon centre ($^1J_{Si,H}$ = 251.7 Hz) [98],

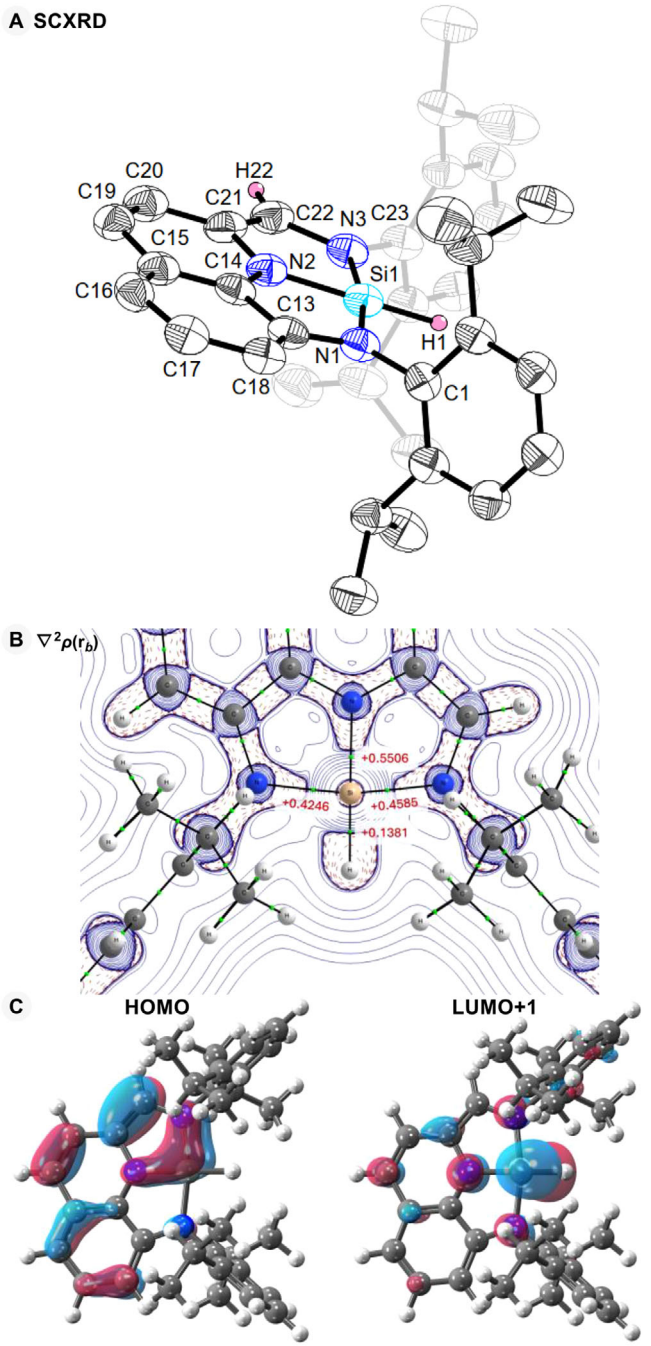

SCHEME 3 | (A): Molecular structure of **Si3** in the crystal. Only the non-disordered molecule is shown. Anisotropic displacement parameters are drawn at the 50% probability level (hydrogen atoms, except for H1 and H22 have been omitted for clarity) Selected bond lengths (Å) and angles (deg): Si1–N1 1.797(4), Si1–N2 1.747(5), Si1–N3 1.784(4), Si1–H1 1.38(4), N1–C13 1.401(6), C13–C14 1.396(7), C13–C18 1.390(7), C17–C18 1.401(7), C16–C17 1.392(8), C15–C16 1.399(7), C14–C15 1.395(7), C15–C19 1.456(8), C19–C20 1.349(8), C20–C21 1.443(8), N2–C21 1.381(6), N2–C14 1.354(6), C21–C22 1.363(8), N3–C22 1.396(7), N1–Si1–N3 168.6(2), H1–Si1–N2 177.3(19); (B): Laplacian of the electron density ($\nabla^2\rho(r_b)$) (PBE0/def2-TZVP) map around the core of **Si3** from QTAIM analysis. (C): Selected Kohn-Sham DFT Molecular Orbitals (HOMO and LUMO+1; PBE0/def2-TZVP) of **Si3**.

underscoring the pronounced effect of planarisation at the silicon centre in **Si3**. A second Si,H coupling arises due to coupling to the exocyclic hydrogen atom with respect to the quinolide ligand. Accordingly, the resonance collapses to a singlet upon ^{1}H decoupling. The ^{1}H NMR chemical shift of the Si–H hydrogen atom at $\delta^{1}H = 5.90$ ppm is only marginally different from that of the precursor **Si1** ($\delta^{1}H = 5.89$ ppm) but, consistent with expectations, is shifted markedly upfield relative to the NHC-ligated derivatives **Si2a**,**b** [78]. The UV/vis spectrum of **Si3** in toluene shows strong absorption bands at 431 and 328 nm, a behaviour that contrasts with the typical non-chromophoric nature of tetracoordinated silanes in tetrahedral coordination environment, owing to the changes in band gap and are consistent with the deep yellow colour.

To further shed light on the electronic structure of **Si3**, it was analysed using density functional theory (DFT) at the PBE0/def2-TZVP level of theory [99–103]. Inspection of the frontier Kohn–Sham molecular orbitals show that the silicon atom is embedded in the molecule, bound by both σ and π interactions with the nitrogen atoms. On the latter point, evidence for extensive electron delocalisation across the π manifold of the complex is observed in the HOMO-1 and HOMO, involving each of the two *cis* N–Si–N triads (*cf*. Scheme 3, B and Figure S72). Natural Bond Orbital (NBO) analysis (Figures S73–S75) found a $s^{0.48}p^{0.52}$ silicon NAO contribution to the Si—H bonding [104]. NBO, however, found the Si—N bonds difficult to class within a Lewis structure, which is common with strongly delocalised and aromatic systems, describing all Si—N interactions in the σ manifold as dative interactions with large (>130 kcal•mol^{-1}) interaction energies between the in-plane nitrogen lone pairs and two silicon lone-vacant orbitals. It, however, seemed to better describe the π manifold, agreeing with the frontier MOs and finding a 3-centred-4-electron bond between the quinolide N–Si π-bond and the lone pair of the enamido nitrogen atom. All three Si—N bonds were found to have similar Wiberg Bond Indices (WBI), indicating the same bond order, and Natural Population Analysis (NPA) assigned the enamido and amido nitrogen atoms with effectively the same charge. Thus, this is in favour of a trianionic ligand structure over the imino-quinoline structure seen in the monoanionic ligand.

The NPA charge of Si is +1.50, which is considerably more electron-rich than the monomeric, pyramidalised ($^{i\mathrm{Pr}}$NNN)SiH [94] and square planar calix[4]pyrrolato-silane **IV** [59], both reported by Greb and co-workers (+1.85 and +2.32 respectively). The electron configuration at silicon in **Si3** ([Ne]$3s^{0.72}3p^{1.74}$) also has markedly increased p-character when compared to the literature examples ($^{i\mathrm{Pr}}$NNN)SiH ([Ne]$3s^{0.72}3p^{1.44}$) [94], as well as **IV** ([Ne]$3s^{0.57}3p^{1.05}$) [59].

The electron delocalisation and planar nature of the system led us to investigate whether the system is aromatic, and if so, how aromatic the system is. For this, Nuclear-independent chemical shifts (NICS) were calculated using Banquo atoms situated in the centre of each ring (NICS0), as well as one Å above the plane (NICS1) (Figure S76) [105]. As they are classical aromatic systems, the two Dipp moieties in the molecule were able to provide an internal reference to further validate our analysis. We found that the C_6 half of the quinolide, in addition to the two 6-π-electron C_2N_2Si rings can be considered as aromatic, whilst the C_5N ring is non-aromatic, in agreement with the redox adaptation of the ligand and the spectroscopically obtained data.

Topological analysis using quantum theory of atoms in molecules (QTAIM), calculated using a wavefunction produced at the same level of theory, was also in favour of three similar Si—N bonds. These are described as intermediate interactions, where the bonds cannot be definitively classed as open shell (covalent) nor closed shell (ionic) (Scheme 3, B and Figures S77 and S78) [106, 107]. The Si–H can also be described as such, in line with Bader's observations that silicon hydrides are some of the simplest examples of intermediate interactions [108].

Considering the above data, it would be best to describe **Si3** as an electron rich silane, with a trianionic ligand. The silicon, owing to its low-lying unoccupied p-acceptor orbital, takes part in both σ and π bonding within the aromatic structure.

To gain an additional insight into the effect of structural/geometric constraint on the electronic structure, a theoretical silane was modelled using a bidentate pyridine-imine ligand and a diphenyl amide, thus breaking the ligand into two components which should have very similar donor and acceptor properties at the Si—H moiety. Geometric optimisation at the PBE0/def2-TZVP yielded a tetrahedral silane, even when a square-planar initial geometry is given, allowing for direct comparison of square planar and tetrahedral coordination (Figure S81). In comparison with the broken ligand, **Si3** was found to be more electron rich (NPA +1.50 vs. +1.84), with an electron configuration of [Ne]$3s^{0.72}3p^{1.74}$ vs. [Ne]$3s^{0.71}3p^{1.40}$, in line with the literature examples, vide supra. The hydride, by its charge and bonding metrics, does not change significantly between the two structures, that is, there is no indication that the hydride will be more or less reactive. Some differences, owing to though the incorporation of the silicon into the ligands π system in **Si3,** are however seen in both the NBO and QTAIM analysis. In the NBO analysis, the NAO composition at silicon changes from $s^{0.48}p^{0.52}$ to $s^{0.32}p^{0.68}$, and all three Si—N bonds are described as 2-centred-2-electron bonds. In the topological analysis, there is an increased bond ellipticity in **Si3** (0.17), compared to 0.03 for the broken system, indicating that the π system strays out towards the H (rather than the Si–H bond having π character), though it must be noted that aromatic C–H bonds show negligible bond ellipticity.

Notably, the accessibility of the silicon-centred p-type orbital (LUMO+1) (*cf*. Scheme 3, C) was experimentally corroborated by the clean reaction of **Si3** with $I^{i}Pr_2Me_2$, which cleanly yielded the corresponding NHC-stabilised silane **Si2b** (Scheme 2) [78]. In this context, and given that **Si3** was crystallised from a THF-containing mixture, we considered whether the relatively weak donor THF might also coordinate to the silicon centre of **Si3**. Addition of a slight excess of THF to **Si3** on the NMR scale at room temperature revealed no evidence for THF coordination under these conditions (Figure S45). To rationalise this behaviour, the thermodynamics of THF coordination were evaluated computationally. While the process is enthalpically favourable ($\Delta H = -12.4$ kcal mol^{-1}), ΔG becomes positive at temperatures above −40°C (Table S17). This prediction is in close agreement with variable-temperature ^{1}H NMR experiments (Figures S46 and S47), which indicate that THF coordination is only feasible at temperatures below −40°C under these conditions. This

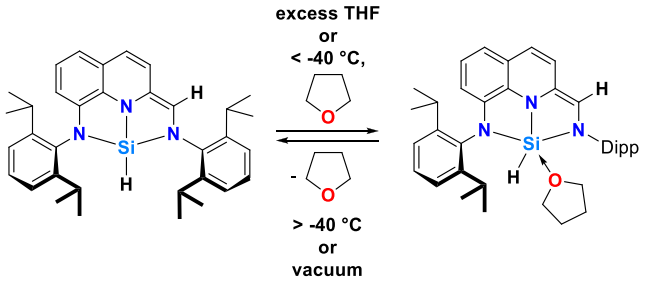

SCHEME 4 | Investigations of reversible THF coordination to **Si3** leading to the formation of the THF adduct **Si3•THF**.

interpretation is further supported by ^{29}Si NMR spectra recorded at −60°C, which exhibit a characteristic upfield shift of approximately 20 ppm relative to **Si3**, consistent with THF adduct formation (Scheme 4 and Figure S48). The same chemical shift is observed when the NMR data of **Si3** are collected in THF-d_8 as the solvent (Figures S49–S53), indicating formation of the corresponding adduct **Si3•THF**. Upon removal of all volatile components under vacuum and redissolution the remaining solid in C_6D_6, only signals corresponding to **Si3** are observed, demonstrating the weak and reversible nature of THF binding to **Si3**.

To further investigate the key hypothesis that a Si(+IV) species supported by a dearomatised ligand can engage in bond activation *via* ELC, while a constant oxidation state at silicon is maintained, **Si3** was reacted with a terminal alkyne derivative, 1-fluoro-4-ethynylbenzene. This reaction resulted in the immediate and quantitative consumption of **Si3**, affording the corresponding formal 1,2-addition product through the addition of the carbon–carbon triple bond across the silicon centre and the exocyclic carbon of the dearomatised quinolide backbone, yielding **Si4** in a regioselective manner (Scheme 2). The successful synthesis of **Si4** was confirmed by multinuclear NMR spectroscopy, LIFDI-MS, IR spectroscopy, and SC-XRD [78]. The analytical data are fully consistent with the herein reported diagnostic features of ligand rearomatisation, including the ^{15}N NMR shifts, as well as other NMR signatures characteristic of a five-coordinate silane retaining a Si—H bond (Scheme 2) [78]. The molecular structure of **Si4**, depicted in Figure 2, represents the first structurally authenticated follow-up product of a square-planar Si(+IV) compound, obtained *via* ELC.

The molecular structure confirms the regioselective carbosilylation of the former alkyne as already evidenced by NMR spectroscopy, with the sterically less demanding terminus bound to the silicon centre. The newly formed Si1—C35 bond length of 1.9061(15) Å is consistent with a typical silicon–carbon single bond and the C35—C36 bond length of 1.3500(18) Å falls within the typical range for alkenes ($\Sigma_{cov,r}$(Si–C) = 1.91 Å; $\Sigma_{cov,r}$(C=C) = 1.34 Å [90, 91]). In accordance with the element–ligand cooperative activation of the substrate, the bond metrics confirm rearomatisation of the quinolide ligand, as evidenced by the homogenised bond lengths across the aromatic framework (Figure 2).

We explored the mechanism of this reaction using DFT and *ab initio* calculations finding that, by making use of the unusual electronics at the square-planar silicon atom, the electrophilic silicon centre first undergoes nucleophilic attack from the alkyne

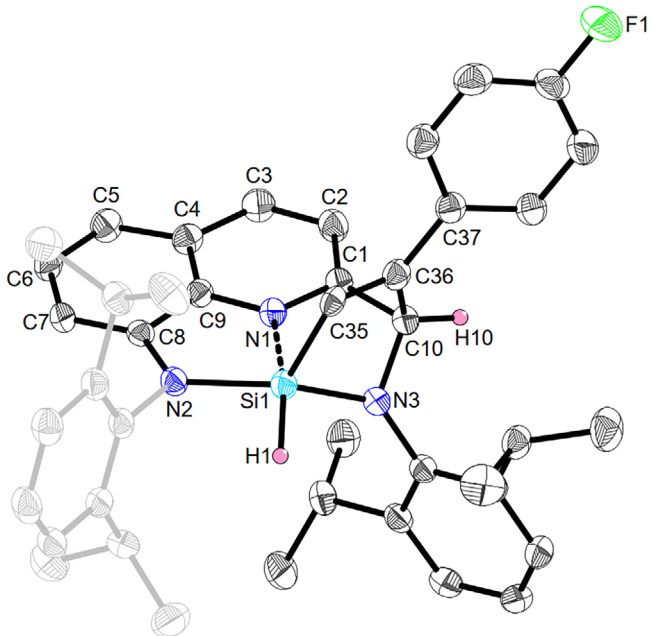

FIGURE 2 | Molecular structure of **Si4** in the crystal. Anisotropic displacement parameters are drawn at the 50% probability level (hydrogen atoms, except for H1 and H10, and disorder have been omitted for clarity). Selected bond lengths (Å) and angles (deg): Si1–C35 1.9061(15), Si1–N1 1.9472(12), Si1–N2 1.8544(12), Si1–N3 1.7955(12), C35–C36 1.3500(18), C1–C10 1.5482(18), N3–C10 1.4719(17), N1–C9 1.3290(16), N1–C1 1.3167(16), C1–C2 1.4058(19), C2–C3 1.3920(19), C3–C4 1.4229(18), C4–C9 1.3992(18), C4–C5 1.4230(18), C5–C6 1.3761(19), C6–C7 1.4254(19), C7–C8 1.3826(18), C8–C9 1.4233(17), N2–C8 1.3870(17), N2–Si1–N3 144.89(5), N2–Si1–C35 117.95(6), N3–Si1–C35 88.30(6), Σ∠N1 359.9, Σ∠N2 359.8, Σ∠N3 360.0.

($\Delta G^{\ddagger}_{298}$ = +7 kcal•mol^{-1}), furnishing a zwitterionic trigonal bipyramidal intermediate **B**, with a carbocationic substituent (ΔG_{298} = +5 kcal•mol^{-1}), consistent with more positive natural (NPA) charge (−0.01 to +0.16) on the internal carbon (Scheme 5). Notably, this is consistent with the observation that the same reaction, when initiated from the NHC-stabilised derivative **Si2b**, does not proceed. This is followed by a nucleophilic attack on the carbocation via the exocyclic carbon, which was shown to be barrierless, yielding the observed product **C** (ΔG_{298} = −20 kcal•mol^{-1}), and reinstating the neutral natural charge on the carbon. During the second process, the quinolide aromatises to a quinoline, providing a driving force for the reaction. The rearomatisation is shown in the IBO analysis, and further supported by NICS0 and NICS1 analysis on stationary points **A**, **B** and **C** (Scheme 5) [109, 110].

3 | Conclusion

In this study, we report the successful synthesis and comprehensive characterisation of a square-planar silicon(+IV) hydride of the type (NNN)SiH (**Si3**), accessed through a concise two-step sequence starting from ligand precursor **L1**, its conversion to the chlorosilane (NNN)Si(H)Cl (**Si1**), and final base-induced dehydrohalogenation. SC-XRD analysis, complementary spectroscopic data, and DFT calculations unambiguously establish the distinctive electronic structure of **Si3**, which is further marked by a non-aromatic ligand backbone. The latter was identified as

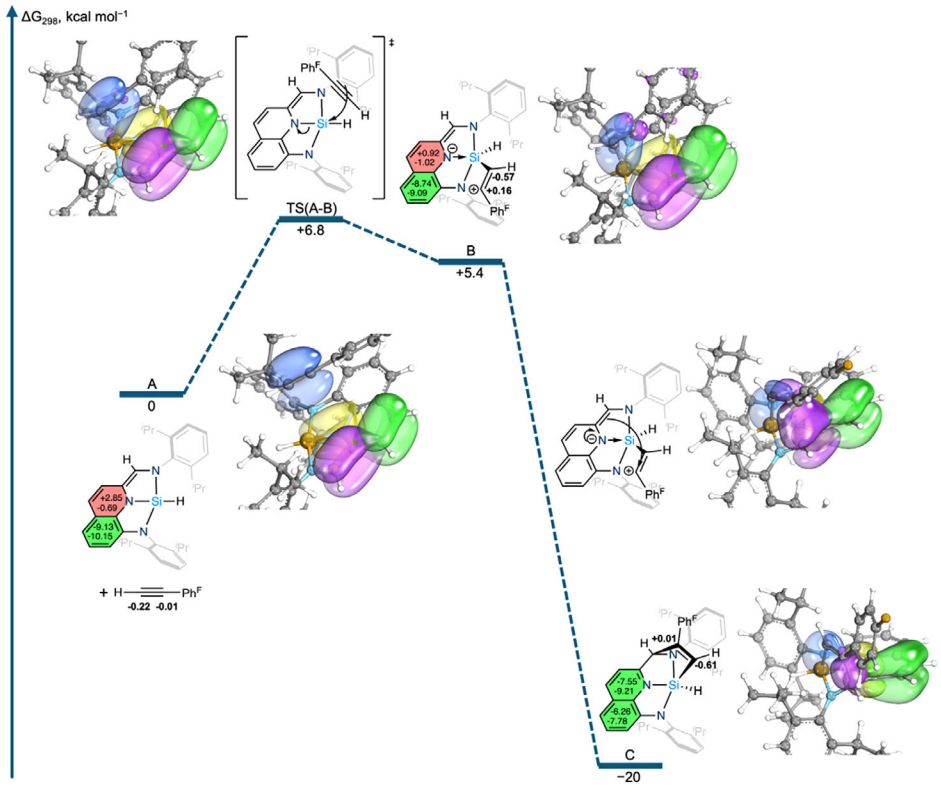

SCHEME 5 | Proposed mechanism for the activation of 1-fluoro-4-ethynylbenzene by **Si3**. Calculated using DFT at the PBE0-D3(BJ)/def2-TZVP (PCM = Benzene) level of theory. Selected orbitals are derived from ab initio intrinsic bond orbital (IBO) analysis performed at the PBE(0)/def2-TZVP level of theory on 38 points across the potential energy surface. Numbers inside rings show NICS0 (top) and NICS1 (bottom) values, with the colour of the ring depicting aromaticity (green) and the absence of (red). Numbers in bold show selected NPA charges.

a key driving force together with the square-planar coordination environment at silicon for the element–ligand-cooperative activation of a terminal alkyne, cleanly affording the corresponding activation product **Si4**, whose structure and formation mechanism were elucidated through quantum-chemical analysis. Isolation of the NHC-stabilised derivatives of **Si3** (**Si2a**,**b**), obtained either via a 2:1 reaction of the respective NHCs with **Si1** under dehydrohalogenation conditions or directly in a 1:1 reaction with **Si3**, revealed additional facets of the system's reactivity. Notably, these NHC-ligated species do not react with the selected terminal alkyne, supporting a mechanistic model in which nucleophilic attack of the alkyne at the silicon centre constitutes the initial step. Accordingly, this pathway is sterically and electronically blocked in the NHC-coordinated derivatives. Such reactivity parallels constant-oxidation-state transformations typically associated with transition metal chemistry and contrasts with dominant paradigms in main-group activation chemistry, which often rely on low-valent species for small-molecule activation. Overall, these findings establish a new structural and mechanistic regime for high-valent silicon, broadening the conceptual landscape of element–ligand cooperativity within the main-group domain.

Acknowledgments

Financial support (VCI Liebig fellowship for O.P.E.T. and M.F.; YIG Prep Pro fellowship for O.P.E.T.) is gratefully acknowledged. Part of the work was funded within the Deutsche Forschungsgemeinschaft (DFG) project SFB 1633, 510228793, project A05. The NMR, MS, and EA services at the Faculty of Chemistry of the Georg-August-Universität Göttingen are kindly acknowledged for measurements and technical assistance. Support from the DFG (INST 186/1237-1 and INST 186/1324-1) is also gratefully acknowledged. M.F. further thanks Prof. Inke Siewert for her continuous support. The authors acknowledge support by the state of Baden–Württemberg through bwHPC and the DFG through grant no INST 40/575-1 FUGG for access to the JUSTUS 2 cluster.

Open access funding enabled and organized by Projekt DEAL.

Conflicts of Interest

The authors declare no conflicts of interest.

Data Availability Statement

All data generated and analysed during this study are included in the published article and the corresponding supplementary material of this article.

References

1. R. L. Parker, "Composition of the Earth's Crust, U.S Geological Survey," (1967).

2. L. Wang, Y. Li, Z. Li, and M. Kira, "Isolable Silylenes and Their Diverse Reactivity," *Coordination Chemistry Reviews* 457 (2022): 214413, https://doi.org/10.1016/j.ccr.2022.214413.

3. M. Denk, R. Lennon, R. Hayashi, et al., "Synthesis and Structure of a Stable Silylene," *Journal of the American Chemical Society* 116 (1994): 2691–2692, https://doi.org/10.1021/ja00085a088.

4. A. C. Filippou, O. Chernov, and G. Schnakenburg, "Si Br_2 (Idipp): A Stable *N*-Heterocyclic Carbene Adduct of Dibromosilylene," *Angewandte*

Chemie International Edition 48 (2009): 5687–5690, https://doi.org/10.1002/anie.200902431.

5. R. S. Ghadwal, H. W. Roesky, S. Merkel, J. Henn, and D. Stalke, "Lewis Base Stabilized Dichlorosilylene," *Angewandte Chemie International Edition* 48 (2009): 5683–5686, https://doi.org/10.1002/anie.200901766.

6. A. V. Protchenko, K. H. Birjkumar, D. Dange, et al., "A Stable Two-Coordinate Acyclic Silylene," *Journal of the American Chemical Society* 134 (2012): 6500–6503, https://doi.org/10.1021/ja301042u.

7. F. Hanusch, L. Groll, and S. Inoue, "Recent Advances of Group 14 Dimetallenes and Dimetallynes in Bond Activation and Catalysis," *Chemical Science* 12 (2001): 2001–2015.

8. R. West, M. J. Fink, and J. Michl, "Tetramesityldisilene, a Stable Compound Containing a Silicon-Silicon Double Bond," *Science* 214 (1981): 1343–1344, https://doi.org/10.1126/science.214.4527.1343.

9. A. Sekiguchi, R. Kinjo, and M. Ichinohe, "A Stable Compound Containing a Silicon-Silicon Triple Bond," *Science* 305 (2004): 1755–1757, https://doi.org/10.1126/science.1102209.

10. S. Stigler, S. Fujimori, A. Kostenko, and S. Inoue, "Tetryliumylidene Ions in Synthesis and Catalysis," *Chemical Science* 15 (2024): 4275–4291, https://doi.org/10.1039/D3SC06452B.

11. P. Jutzi, A. Mix, B. Rummel, W. W. Schoeller, B. Neumann, and H.-G. Stammler, "The $(Me_5C_5)Si^+$ Cation: A Stable Derivative of HSi^+," *Science* 305 (2004): 849–851, https://doi.org/10.1126/science.1099879.

12. A. C. Filippou, Y. N. Lebedev, O. Chernov, M. Straßmann, and G. Schnakenburg, "Silicon(II) Coordination Chemistry: *N*-Heterocyclic Carbene Complexes of Si^{2+} and SiI^+," *Angewandte Chemie International Edition* 52 (2013): 6974–6978, https://doi.org/10.1002/anie.201301363.

13. A. Hinz, "A Mono-Substituted Silicon(II) Cation: A Crystalline "Supersilylene"," *Angewandte Chemie International Edition* 59 (2020): 19065–19069, https://doi.org/10.1002/anie.202009874.

14. P. K. Majhi and T. Sasamori, "Tetrylones: An Intriguing Class of Monoatomic Zero-Valent Group 14 Compounds," *Chemistry–A European Journal* 24 (2018): 9441–9455, https://doi.org/10.1002/chem.201800142.

15. Y. Xiong, S. Yao, S. Inoue, J. D. Epping, and M. Driess, "A Cyclic Silylone ("Siladicarbene") With an Electron-Rich Silicon(0) Atom," *Angewandte Chemie International Edition* 52 (2013): 7147–7150, https://doi.org/10.1002/anie.201302537.

16. K. C. Mondal, H. W. Roesky, M. C. Schwarzer, et al., "A Stable Singlet Biradicaloid Siladicarbene: $(L:)_2Si$," *Angewandte Chemie International Edition* 52 (2013): 2963–2967, https://doi.org/10.1002/anie.201208307.

17. T. J. Hadlington, "Heavier Tetrylene- and Tetrylyne-transition Metal Chemistry: It's no Carbon Copy," *Chemical Reviews* 53 (2025): 9738.

18. H. F. T. Klare, L. Albers, L. Süsse, S. Keess, T. Müller, and M. Oestreich, "Silylium Ions: From Elusive Reactive Intermediates to Potent Catalysts," *Chemical Reviews* 121 (2021): 5889–5985, https://doi.org/10.1021/acs.chemrev.0c00855.

19. C. Shan, S. Yao, and M. Driess, "Where Silylene–silicon Centres Matter in the Activation of Small Molecules," *Chemical Society Reviews* 49 (2020): 6733–6754, https://doi.org/10.1039/D0CS00815J.

20. B. Shao, A. L. Bagdasarian, S. Popov, and H. M. Nelson, "Arylation of Hydrocarbons Enabled by Organosilicon Reagents and Weakly Coordinating Anions," *Science* 355 (2017): 1403–1407, https://doi.org/10.1126/science.aam7975.

21. M. Hirai, N. Tanaka, M. Sakai, and S. Yamaguchi, "Structurally Constrained Boron-, Nitrogen-, Silicon-, and Phosphorus-Centered Polycyclic π-Conjugated Systems," *Chemical Reviews* 119 (2019): 8291–8331, https://doi.org/10.1021/acs.chemrev.8b00637.

22. T. J. Hannah and S. S. Chitnis, "Ligand-Enforced Geometric Constraints and Associated Reactivity in p-block Compounds," *Chemical Society Reviews* 53 (2024): 764–792, https://doi.org/10.1039/D3CS00765K.

23. H. Ruppert, L. M. Sigmund, and L. Greb, "Calix[4]Pyrroles as Ligands: Recent Progress With a Focus on the Emerging p-Block Element Chemistry," *Chemical Communications* 57 (2021): 11751–11763, https://doi.org/10.1039/D1CC05120B.

24. J. Abbenseth and J. M. Goicoechea, "Recent Developments in the Chemistry of Non-Trigonal Pnictogen Pincer Compounds: From Bonding to Catalysis," *Chemical Science* 11 (2020): 9728–9740, https://doi.org/10.1039/D0SC03819A.

25. S. G. Nelson, B.-K. Kim, and T. J. Peelen, "Lewis Acidity Expressed in Neutral Electron-Rich Aluminum(III) Complexes: An Example of Ligand-Defined Catalysis," *Journal of the American Chemical Society* 122 (2000): 9318–9319, https://doi.org/10.1021/ja002415q.

26. E. J. Thompson, T. W. Myers, and L. A. Berben, "Synthesis of Square-Planar Aluminum(III) Complexes," *Angewandte Chemie International Edition* 53 (2014): 14132–14134, https://doi.org/10.1002/anie.201407098.

27. A. Ben Saida, A. Chardon, A. Osi, et al., "Pushing the Lewis Acidity Boundaries of Boron Compounds With Non-Planar Triarylboranes Derived From Triptycenes," *Angewandte Chemie International Edition* 58 (2019): 16889.

28. M.-H. Wang, C. Chen, S. Pan, and Z.-H. Cui, "Planar Hexacoordinate Gallium," *Chemical Science* 12 (2021): 15067–15076, https://doi.org/10.1039/D1SC05089C.

29. A. Osi, D. Mahaut, N. Tumanov, et al., "Taming the Lewis Superacidity of Non-Planar Boranes: C−H Bond Activation and Non-Classical Binding Modes at Boron," *Angewandte Chemie International Edition* 61 (2022): e202112342, https://doi.org/10.1002/anie.202112342.

30. L. M. Sigmund, E. Engels, N. Richert, and L. Greb, "Calix[4]Pyrrolato Gallate: Square Planar-coordinated Gallium(iii) and Its Metal–ligand Cooperative Reactivity With CO_2 and Alcohols," *Chemical Science* 13 (2022): 11215–11220, https://doi.org/10.1039/D2SC03054C.

31. W. Lv, Y. Dai, R. Guo, et al., "Geometrically Constrained Organoboron Species as Lewis Superacids and Organic Superbases," *Angewandte Chemie International Edition* 62 (2023): e202308467, https://doi.org/10.1002/anie.202308467.

32. N. L. Dunn, M. Ha, and A. T. Radosevich, "Main Group Redox Catalysis: Reversible P III /P V Redox Cycling at a Phosphorus Platform," *Journal of the American Chemical Society* 134 (2012): 11330–11333, https://doi.org/10.1021/ja302963p.

33. T. P. Robinson, D. M. De Rosa, S. Aldridge, and J. M. Goicoechea, "E–H Bond Activation of Ammonia and Water by a Geometrically Constrained Phosphorus(III) Compound," *Angewandte Chemie International Edition* 54 (2015): 13758–13763, https://doi.org/10.1002/anie.201506998.

34. A. Hentschel, A. Brand, P. Wegener, and W. Uhl, "A Sterically Constrained Tricyclic PC_3 Phosphine: Coordination Behavior and Insertion of Chalcogen Atoms Into P−C Bonds," *Angewandte Chemie International Edition* 57 (2018): 832–835, https://doi.org/10.1002/anie.201711373.

35. S. Volodarsky and R. Dobrovetsky, "Ambiphilic Geometrically Constrained Phosphenium Cation," *Chemical Communications* 54 (2018): 6931–6934, https://doi.org/10.1039/C8CC02423E.

36. M. B. Kindervater, K. M. Marczenko, U. Werner-Zwanziger, and S. S. Chitnis, "A Redox-Confused Bismuth(I/III) Triamide With a T-Shaped Planar Ground State," *Angewandte Chemie International Edition* 58 (2019): 7850–7855, https://doi.org/10.1002/anie.201903354.

37. J. Abbenseth, O. P. E. Townrow, and J. M. Goicoechea, "Thermoneutral N−H Bond Activation of Ammonia by a Geometrically Constrained Phosphine," *Angewandte Chemie International Edition* 60 (2021): 23625–23629, https://doi.org/10.1002/anie.202111017.

38. S. Volodarsky, D. Bawari, and R. Dobrovetsky, "Dual Reactivity of a Geometrically Constrained Phosphenium Cation," *Angewandte Chemie International Edition* 61 (2022): e202208401, https://doi.org/10.1002/anie.202208401.

39. M. Schorpp, R. Yadav, D. Roth, and L. Greb, "Calix[4]Pyrrolato Stibenium: Lewis Superacidity by Antimony(III)-Antimony(V) Electromerism," *Angewandte Chemie International Edition* 61 (2022): e202207963, https://doi.org/10.1002/anie.202207963.

40. S. Volodarsky, I. Malahov, D. Bawari, et al., "Geometrically Constrained Square Pyramidal Phosphoranide," *Chemical Science* 13 (2022): 5957–5963, https://doi.org/10.1039/D2SC01060G.

41. K. Chulsky, I. Malahov, D. Bawari, and R. Dobrovetsky, "Metallomimetic Chemistry of a Cationic, Geometrically Constrained Phosphine in the Catalytic Hydrodefluorination and Amination of Ar–F Bonds," *Journal of the American Chemical Society* 145 (2023): 3786–3794, https://doi.org/10.1021/jacs.2c13318.

42. T. J. Hannah, W. M. McCarvell, T. Kirsch, et al., "Planar Bismuth Triamides: A Tunable Platform for Main Group Lewis Acidity and Polymerization Catalysis," *Chemical Science* 14 (2023): 4549–4563, https://doi.org/10.1039/D3SC00917C.

43. T. J. Hannah, T. Z. Kirsch, and S. S. Chitnis, "Why Are some Pnictogen(III) Pincer Complexes Planar and Others Pyramidal?," *Chemistry–A European Journal* 30 (2024): e202402851, https://doi.org/10.1002/chem.202402851.

44. D. Bawari, D. Toami, K. Jaiswal, and R. Dobrovetsky, "Hydrogen Splitting at a Single Phosphorus Centre and Its Use for Hydrogenation," *Nature Chemistry* 16 (2024): 1261–1266, https://doi.org/10.1038/s41557-024-01569-y.

45. S. Pavlidis, C. Teutloff, A. G. Buzanich, et al., "A Crystalline Bismuth(II) Radical Anion: Synthesis, Characterization, and Reactivity," *Angewandte Chemie International Edition* 64 (2025): e202515545, https://doi.org/10.1002/anie.202515545.

46. H. Ruppert and L. Greb, "Calix[4]Pyrrolato Stannate(II): A Tetraamido Tin(II) Dianion and Strong Metal-Centered σ-Donor," *Angewandte Chemie International Edition* 61 (2022): e202116615, https://doi.org/10.1002/anie.202116615.

47. R. Yadav, P. Janßen, M. Schorpp, and L. Greb, "Calix[4]Pyrrolatogermane-(thf) 2: Unlocking the Anti-van't Hoff–Le Bel Reactivity of Germanium(IV) by Ligand Dissociation," *Journal of the American Chemical Society* 145 (2023): 17746–17754, https://doi.org/10.1021/jacs.3c04424.

48. C. Shan, S. Dong, S. Yao, J. Zhu, and M. Driess, "Synthesis and Reactivity of an Anti-van't Hoff/Le Bel Compound With a Planar Tetracoordinate Silicon(II) Atom," *Journal of the American Chemical Society* 145 (2023): 7084–7089, https://doi.org/10.1021/jacs.3c00722.

49. X. Liu, Y. Dai, M. Bao, et al., "A Crystalline T-shaped Planar Group 14 Anion," *Chemical Science* 14 (2023): 5722–5727, https://doi.org/10.1039/D2SC07006E.

50. H. Ruppert, A. Meister, R. Pfretzschner, A. F. Vieira, and L. Greb, "Concatenating Structural Constraint Effects at Tin for the Sequential Generation, Stabilization, and Transfer of Acyclic Aminocarbenes," *Journal of the American Chemical Society* 146 (2024): 11515–11522, https://doi.org/10.1021/jacs.4c02446.

51. H. Ruppert, T. Schreyer, M. C. Dietl, M. Rudolph, S. K. Hashmi, and L. Greb, "Dynamic Coordination Behavior of a Structurally Constrained, Nucleophilic Sn(II) toward Gold(I)," *Zeitschrift für anorganische und allgemeine Chemie* 650 (2024): e202400081, https://doi.org/10.1002/zaac.202400081.

52. X. Liu, Y. Dai, Q. Bao, et al., "Isolable T-Shaped Planar Silyl Anion," *Angewandte Chemie International Edition* 63 (2024): e202406089, https://doi.org/10.1002/anie.202406089.

53. P. A. B. Latigua, M. Lutz, and M.-E. Moret, "Polar X–H Bond (X = O, S, N) Activation at a Cage Silanide," *Angewandte Chemie International Edition* 136 (2024): e202319899.

54. V. D. Hannibal and L. Greb, "Tetra-Amido Macrocyclic Ligand (TAML) at Silicon(IV): A Structurally Constrained, Water-Soluble Silicon Lewis Superacid," *Journal of the American Chemical Society* 146 (2024): 25727–25737, https://doi.org/10.1021/jacs.4c08015.

55. A. I. Boldyrev, X. Li, and L. S. Wang, "Experimental Observation of Pentaatomic Tetracoordinate Planar Si- and Ge-Containing Molecules: MAl 4- and MAl 4," *Angewandte Chemie International Edition* 39 (2000): 3307–3310, https://doi.org/10.1002/1521-3773(20000915)39:18%3c3307::AID-ANIE3307%3e3.0.CO;2-.

56. M. J. Cowley, V. Huch, and D. Scheschkewitz, "Donor–Acceptor Adducts of a 1,3-Disila-2-oxyallyl Zwitterion," *Chemistry–A European Journal* 20 (2014): 9221–9224, https://doi.org/10.1002/chem.201402750.

57. T. Nukazawa and T. Iwamoto, "An Isolable Tetrasilicon Analogue of a Planar Bicyclo[1.1.0]Butane With π-Type Single-Bonding Character," *Journal of the American Chemical Society* 142 (2020): 9920–9924, https://doi.org/10.1021/jacs.0c03874.

58. P. Ghana, J. Rump, G. Schnakenburg, M. I. Arz, and A. C. Filippou, "Planar Tetracoordinated Silicon (ptSi): Room-Temperature Stable Compounds Containing Anti-van't Hoff/Le Bel Silicon," *Journal of the American Chemical Society* 143 (2021): 420–432, https://doi.org/10.1021/jacs.0c11628.

59. F. Ebner and L. Greb, "An Isolable, Crystalline Complex of Square-planar Silicon(IV)," *Chemistry* 7 (2021): 2151–2159, https://doi.org/10.1016/j.chempr.2021.05.002.

60. J. D. Dunitz, "Planar Four-Coordinated Silicon?," *Angewandte Chemie International Edition* 19 (1980): 1034, https://doi.org/10.1002/anie.198010341.

61. G. Nagorsen and H. Meyer, "Planar Four-Coordinated Silicon—A Reply," *Angewandte Chemie International Edition* 19 (1980): 1034, https://doi.org/10.1002/anie.198010342.

62. M. B. Krogh-Jespersen, J. Chandrasekhar, E. U. Wuerthwein, J. B. Collins, and P. Von Ragué Schleyer, "Molecular Orbital Study of Tetrahedral, Planar, and Pyramidal Structures of the Isoelectronic Series BH_4^-, CH_4, NH_4^+, AlH_4^-, SiH_4, and PH_4^+," *Journal of the American Chemical Society* 102 (1980): 2263–2268, https://doi.org/10.1021/ja00527a021.

63. C. Gunanathan and D. Milstein, "Metal–Ligand Cooperation by Aromatization–Dearomatization: A New Paradigm in Bond Activation and "Green" Catalysis," *Accounts of Chemical Research* 44 (2011): 588–602, https://doi.org/10.1021/ar2000265.

64. J. R. Khusnutdinova and D. Milstein, "Bond Activation and Catalysis by Ruthenium Pincer Complexes," *Chemical Reviews* 114 (2014): 12024.

65. M. R. Elsby and R. T. Baker, "Strategies and Mechanisms of Metal–ligand Cooperativity in First-Row Transition Metal Complex Catalysts," *Chemical Society Reviews* 49 (2020): 8933–8987, https://doi.org/10.1039/D0CS00509F.

66. Y. Liang, U. K. Das, J. Luo, Y. Diskin-Posner, L. Avram, and D. Milstein, "Magnesium Pincer Complexes and Their Applications in Catalytic Semihydrogenation of Alkynes and Hydrogenation of Alkenes: Evidence for Metal–Ligand Cooperation," *Journal of the American Chemical Society* 144 (2022): 19115–19126, https://doi.org/10.1021/jacs.2c08491.

67. Y. Liang, J. Luo, Y. Diskin-Posner, and D. Milstein, "Designing New Magnesium Pincer Complexes for Catalytic Hydrogenation of Imines and *N*-Heteroarenes: H_2 and N–H Activation by Metal–Ligand Cooperation as Key Steps," *Journal of the American Chemical Society* 145 (2023): 9164–9175, https://doi.org/10.1021/jacs.3c01091.

68. Y. Liang, I. Efremenko, Y. Diskin-Posner, L. Avram, and D. Milstein, "Calcium-Ligand Cooperation Promoted Activation of N_2O, Amine, and H_2 as Well as Catalytic Hydrogenation of Imines, Quinoline, and Alkenes," *Angewandte Chemie International Edition* 63 (2024): e202401702, https://doi.org/10.1002/anie.202401702.

69. L.-M. Yang, E. Ganz, Z. Chen, Z.-X. Wang, and P. V. R. Schleyer, "Four Decades of the Chemistry of Planar Hypercoordinate Compounds," *Angewandte Chemie International Edition* 54 (2015): 9468–9501, https://doi.org/10.1002/anie.201410407.

70. F. Ebner and L. Greb, "Calix[4]Pyrrole Hydridosilicate: The Elusive Planar Tetracoordinate Silicon Imparts Striking Stability to Its Anionic Silicon Hydride," *Journal of the American Chemical Society* 140 (2018): 17409–17412, https://doi.org/10.1021/jacs.8b11137.

71. Y. Li, F. Li, Z. Zhou, and Z. Chen, "SiC_2 silagraphene and Its One-dimensional Derivatives: Where Planar Tetracoordinate Silicon Happens," *Journal of the American Chemical Society* 133 (2011): 900–908, https://doi.org/10.1021/ja107711m.

72. M. J. Sun, X. Cao, and Z. Cao, "Stabilization of Planar Tetra-coordinate Silicon in a 2D-layered Extended System and Design of a High-Capacity Anode Material for Li-Ion Batteries," *Nanoscale* 10 (2018): 10450–10458, https://doi.org/10.1039/C8NR03566K.

73. Y. Wang, Y. Li, and Z. Chen, "Planar Hypercoordinate Motifs in Two-Dimensional Materials," *Accounts of Chemical Research* 53 (2020): 887–895, https://doi.org/10.1021/acs.accounts.0c00025.

74. Y. Zhang, C. Zhang, Y. Mo, and Z. Cao, "Planar Tetracoordinate Silicon in Organic Molecules as Carbenoid-Type Amphoteric Centers: A Computational Study," *Chemistry–A European Journal* 27 (2021): 1402–1409, https://doi.org/10.1002/chem.202004298.

75. E. U. Würthwein and P. von Ragué Schleyer, "Planar Tetracoordinate Silicon," *Angewandte Chemie International Edition* 18 (1979): 553–554, https://doi.org/10.1002/anie.197905531.

76. S. G. Kim, J. Oh, D. Kim, D. E. Choi, and S. J. Hwang, "Phosphorus-Ligand Redox Cooperative Catalysis: Unraveling Four-Electron Dioxygen Reduction Pathways and Reactive Intermediates," *Journal of the American Chemical Society* 146 (2024): 11440.

77. S. G. Kim, J. Oh, D. Kim, D. E. Choi, and S. J. Hwang, "Direct O_2 Activation by Ligand-Constrained Pnictogen Complexes: Contrasting Mechanisms and OAT Reactivity Across the P, Sb, and Bi Triad," *JACS Au* 5 (2025): 2779–2791, https://doi.org/10.1021/jacsau.5c00371.

78. See the *Supporting Information*.

79. R. Jambor and A. Lyčka, "Organosilicon and -Germanium Hydrides in Catalyst-Free Hydrometallation Reactions," *European Journal of Inorganic Chemistry* 2017 (2017): 4887–4898, https://doi.org/10.1002/ejic.201700630.

80. S. S. Sen, H. W. Roesky, D. Stern, J. Henn, and D. Stalke, "High Yield Access to Silylene RSiCl (R = PhC(N*t*Bu)$_2$) and Its Reactivity Toward Alkyne: Synthesis of Stable Disilacyclobutene," *Journal of the American Chemical Society* 132 (2010): 1123–1126, https://doi.org/10.1021/ja9091374.

81. Y. Xiong, S. Yao, A. Kostenko, and M. Driess, "An Isolable β-diketiminato Chlorosilylene," *Dalton Transactions* 47 (2018): 2152–2155, https://doi.org/10.1039/C8DT00121A.

82. H. T. Dieck and M. Zettlitzer, "Darstellung und Reaktionen N-Silylierter En-Diamine, II [2 + 2]-Cycloadditionen: Synthese von 1,4-Diamino-1,3-Butadien-2,3-Dicarbonsäure-Derivaten," *Chemische Berichte* 120 (1987): 795–801, https://doi.org/10.1002/cber.19871200518.

83. J. Oetzel, C. Bruhn, and U. Siemeling, "On the Way to N-Heterocyclic Silylenes With a 1,1′-Ferrocenediyl Backbone: Synthesis and Structures of Silicon(IV) Compounds of the Type [Fe{(η^5-C_5H_4)NR}$_2$SiX$_2$]," *Zeitschrift für anorganische und allgemeine Chemie* 644 (2018): 935–944, https://doi.org/10.1002/zaac.201800152.

84. P. J. Larkin, *Infrared and Raman Spectroscopy: Principles and Spectral Interpretation* (Elsevier, 2011).

85. V. Nesterov, D. Reiter, P. Bag, et al., "NHCs in Main Group Chemistry," *Chemical Reviews* 118 (2018): 9678–9842, https://doi.org/10.1021/acs.chemrev.8b00079.

86. S. S. Sen, S. Khan, P. P. Samuel, and H. W. Roesky, "Chemistry of Functionalized Silylenes," *Chemical Science* 3 (2012): 659–682, https://doi.org/10.1039/C1SC00757B.

87. G. Dübeck, F. Hanusch, and S. Inoue, "NHC-Stabilized Silyl-Substituted Chlorosilylene," *Inorganic Chemistry* 58 (2019): 15700.

88. C. Eisenhut, T. Szilvási, G. Dübek, N. C. Breit, and S. Inoue, "Systematic Study of *N*-Heterocyclic Carbene Coordinate Hydrosilylene Transition-Metal Complexes," *Inorganic Chemistry* 56 (2017): 10061–10069, https://doi.org/10.1021/acs.inorgchem.7b01541.

89. A. W. Addison, T. N. Rao, J. Reedijk, J. van Rijn, and G. C. Verschoor, "Synthesis, Structure, and Spectroscopic Properties of Copper(II) Compounds Containing Nitrogen–Sulphur Donor Ligands; the Crystal and Molecular Structure of Aqua[1,7-bis(N-methylbenzimidazol-2′-yl)-2,6-dithiaheptane]Copper(II) Perchlorate," *Journal of the Chemical Society, Dalton Transactions* (1984): 1349–1356, https://doi.org/10.1039/DT9840001349.

90. P. Pyykkö and M. Atsumi, "Molecular Single-Bond Covalent Radii for Elements 1–118," *Chemistry–A European Journal* 15 (2009): 186.

91. P. Pyykkö and M. Atsumi, "Molecular Double-Bond Covalent Radii for Elements Li–E112," *Chemistry–A European Journal* 15 (2009): 12770.

92. L. Yang, D. R. Powell, and R. P. Houser, "Structural Variation in Copper(I) Complexes With Pyridylmethylamide Ligands: Structural Analysis With a New Four-coordinate Geometry Index, τ_4," *Dalton Transactions* 955 (2007): 955–964.

93. A. Okuniewski, D. Rosiak, J. Chojnacki, and B. Becker, "Coordination Polymers and Molecular Structures Among Complexes of Mercury(II) Halides With Selected 1-benzoylthioureas," *Polyhedron* 90 (2015): 47–57, https://doi.org/10.1016/j.poly.2015.01.035.

94. N. Kramer, C. Jöst, A. Mackenroth, and L. Greb, "Synthesis of Electron-Rich, Planarized Silicon(IV) Species and a Theoretical Analysis of Dimerizing Aminosilanes," *Chemistry–A European Journal* 23 (2017): 17764–17774, https://doi.org/10.1002/chem.201703649.

95. S. Bachmann, R. Neufeld, M. Dzemski, and D. Stalke, "New External Calibration Curves (ECCs) for the Estimation of Molecular Weights in Various Common NMR Solvents," *Chemistry–A European Journal* 22 (2016): 8462–8465, https://doi.org/10.1002/chem.201601145.

96. S. Bachmann, B. Gernert, and D. Stalke, "Solution Structures of Alkali Metal Cyclopentadienides in THF Estimated by ECC-DOSY NMR-Spectroscopy (incl. Software)," *Chemical Communications* 52 (2016): 12861–12864, https://doi.org/10.1039/C6CC07273A.

97. See for example Table 1: F. Feige, L. A. Malaspina, F. Kleemiss, et al., "An Investigation Into the Brønsted Acidity of the Perfluorinated Alkoxy Silanes {(F_3 C)$_3$ CO}$_3$ SiH and {(F_6C_5)$_3$ CO}$_2$ Si(Cl)H," *Dalton Transactions* 52 (2023): 5918–5925, https://doi.org/10.1039/D3DT00299C.

98. A. Jana, C. Schulzke, and H. W. Roesky, "Oxidative Addition of Ammonia at a Silicon(II) Center and an Unprecedented Hydrogenation Reaction of Compounds With Low-Valent Group 14 Elements Using Ammonia Borane," *Journal of the American Chemical Society* 131 (2009): 4600–4601, https://doi.org/10.1021/ja900880z.

99. J. P. Perdew, K. Burke, and M. Ernzerhof, "Generalized Gradient Approximation Made Simple," *Physical Review Letter* 77 (1996): 3865–3868, https://doi.org/10.1103/PhysRevLett.77.3865.

100. C. Adamo and V. Barone, "Toward Reliable Density Functional Methods Without Adjustable Parameters: The PBE0 Model," *Journal of Chemical Physics* 110 (1999): 6158–6170, https://doi.org/10.1063/1.478522.

101. F. Weigend and R. Ahlrichs, "Balanced Basis Sets of Split Valence, Triple Zeta Valence and Quadruple Zeta Valence Quality for H to Rn: Design and Assessment of Accuracy," *Physical Chemistry Chemical Physics* 7 (2005): 3297, https://doi.org/10.1039/b508541a.

102. S. Grimme, J. Antony, S. Ehrlich, and H. Krieg, "A Consistent and Accurate ab Initio Parametrization of Density Functional Dispersion Correction (DFT-D) for the 94 Elements H-Pu," *Journal of Chemical Physics* 132 (2010): 154104, https://doi.org/10.1063/1.3382344.

103. S. Grimme, S. Ehrlich, and L. Goerigk, "Effect of the Damping Function in Dispersion Corrected Density Functional Theory," *Journal of Computational Chemistry* 32 (2011): 1456–1465, https://doi.org/10.1002/jcc.21759.

104. E. D. Glendening, J. K. Badenhoop, A. E. Reed, and J. E. Carpenter, *NBO 7.0* (Theoretical Chemistry Institute, University of Wisconsin, 2018).

105. Z. Chen, C. S. Wannere, C. Corminboeuf, R. Puchta, and P. V. R. Schleyer, "Nucleus-Independent Chemical Shifts (NICS) as an Aromaticity Criterion," *Chemical Reviews* 105 (2005): 3842–3888, https://doi.org/10.1021/cr030088+.

106. AIMAll (Version 19.10.12), T. A. Keith, TK Gristmill Software, 2019 (aim.tkgristmill.com).

107. P. L. A. Popelier, *The QTAIM Perspective of Chemical Bonding in The Chemical Bond 271–308*,(John Wiley & Sons, Ltd 2014).

108. R. F. W. Bader and H. Essén, "The Characterization of Atomic Interactions," *Journal of Chemical Physics* 80 (1984): 1943–1960, https://doi.org/10.1063/1.446956.

109. G. Knizia, "Intrinsic Atomic Orbitals: An Unbiased Bridge Between Quantum Theory and Chemical Concepts," *Journal of Chemical Theory and Computation* 9 (2013): 4834–4843, https://doi.org/10.1021/ct400687b.

110. G. Knizia and J. E. M. N. Klein, "Electron Flow in Reaction Mechanisms—Revealed From First Principles," *Angewandte Chemie International Edition* 54 (2015): 5518–5522, https://doi.org/10.1002/anie.201410637.

111. C. Barnett, M. L. Cole, and J. B. Harper, "Steric Properties of N-Heterocyclic Carbenes Affect the Performance of Electronic Probes," *European Journal of Inorganic Chemistry* 2021 (2021): 4954–4958, https://doi.org/10.1002/ejic.202100796.

112. N. Kuhn and T. Kratz, "Synthesis of Imidazol-2-ylidenes by Reduction of Imidazole-2(3*H*)-thiones," *Synthesis* 1993 (1993): 561–562, https://doi.org/10.1055/s-1993-25902.

113. M. Fischer and M. Schmidtmann, "$B(C_6F_5)_3$- and $HB(C_6F_5)_2$-Mediated Transformations of Isothiocyanates," *Chemical Communications* 56 (2020): 6205–6208, https://doi.org/10.1039/D0CC02626C.

114. O. Lavinda, C. H. Witt, and K. A. Woerpel, "Origin of High Diastereoselectivity in Reactions of Seven-Membered-Ring Enolates," *Angewandte Chemie International Edition* 61 (2022): e202114183, https://doi.org/10.1002/anie.202114183.

115. G. R. Fulmer, A. J. M. Miller, N. H. Sherden, et al., "NMR Chemical Shifts of Trace Impurities: Common Laboratory Solvents, Organics, and Gases in Deuterated Solvents Relevant to the Organometallic Chemist," *Organometallics* 29 (2010): 2176–2179, https://doi.org/10.1021/om100106e.

116. Bruker AXS Inc., *Saint v8.40B*, Madison, WI, USA, 2019.

117. L. Krause, R. Herbst-Irmer, G. M. Sheldrick, and D. Stalke, "Comparison of Silver and Molybdenum Microfocus X-ray Sources for Single-Crystal Structure Determination," *Journal of Applied Crystallography* 48 (2015): 3–10, https://doi.org/10.1107/S1600576714022985.

118. M. Sevvana, M. Ruf, I. Usón, G. M. Sheldrick, and R. Herbst-Irmer, "Non-Merohedral Twinning: From Minerals to Proteins," *Acta Crystallographica* D75 (2019): 1040.

119. G. M. Sheldrick, "*SHELXT*—Integrated Space-group and Crystal-Structure Determination," *Acta Crystallographica* 71 (2015): 3.

120. G. M. Sheldrick, "Crystal Structure Refinement With SHELXL," *Acta Crystallographica* C71 (2015): 3.

121. O. V. Dolomanov, L. J. Bourhis, R. J. Gildea, J. A. K. Howard, and H. Puschmann, "*OLEX2*: A Complete Structure Solution, Refinement, and Analysis Program," *Journal of Applied Crystallography* 42 (2009): 339–341, https://doi.org/10.1107/S0021889808042726.

122. C. B. Hübschle, G. M. Sheldrick, and B. Dittrich, "ShelXle: A Qt Graphical User Interface for SHELXL," *Journal of Applied Crystallography* 44 (2011): 1281–1284, https://doi.org/10.1107/S0021889811043202.

123. D. Kratzert, FinalCif, V132, https://dkratzert.de/finalcif.html.

124. C. R. Groom, I. J. Bruno, M. P. Lightfoot, and S. C. Ward, "The Cambridge Structural Database," *Acta Crystallographica* B72 (2016): 171.

125. S. Parsons, H. Flack, and T. Wagner, "Use of Intensity Quotients and Differences in Absolute Structure Refinement," *Acta Crystallographica* B69 (2013): 249.

126. M. J. Frisch, G. W. Trucks, H. B. Schlegel, et al., (Gaussian, Inc, 2016).

127. F. Neese, "Software Update: The ORCA Program System—Version 6.0," *Molecular Sciences* 15 (2025): e70019, https://doi.org/10.1002/wcms.70019.

128. F. Neese and G. Olbrich, "Efficient Use of the Resolution of the Identity Approximation in Time-Dependent Density Functional Calculations With Hybrid Density Functionals," *Chemical Physics Letters* 362 (2002): 170–178, https://doi.org/10.1016/S0009-2614(02)01053-9.

129. F. Neese, "The SHARK Integral Generation and Digestion System," *Journal of Computational Chemistry* 44 (2022): 381–396, https://doi.org/10.1002/jcc.26942.

130. E. Caldeweyher, J.-M. Mewes, S. Ehlert, and S. Grimme, "Extension and Evaluation of the D4 London-Dispersion Model for Periodic Systems," *Physical Chemistry Chemical Physics* 22 (2020): 8499–8512, https://doi.org/10.1039/D0CP00502A.

131. P. Pollak and F. Weigend, "Segmented Contracted Error-Consistent Basis Sets of Double- and Triple-ζ Valence Quality for One- and Two-Component Relativistic All-Electron Calculations," *Journal of Chemical Theory and Computation* 13 (2017): 3696–3705, https://doi.org/10.1021/acs.jctc.7b00593.

132. Y. J. Franzke, R. Treß, T. M. Pazdera, and F. Weigend, "Error-Consistent Segmented Contracted All-Electron Relativistic Basis Sets of Double- and Triple-Zeta Quality for NMR Shielding Constants," *Physical Chemistry Chemical Physics* 21 (2019): 16658–16664.

Supporting Information

Additional supporting information can be found online in the Supporting Information section.

Detailed descriptions of experimental, spectroscopic, crystallographic and quantum chemical methods and results are given in the Supporting Information. The structures of **L1**, **Si2b**, **Si3** and **Si4** were determined by SC-XRD. Crystallographic data of the structures reported in this article have been deposited at the Cambridge Crystallographic Data Centre, under deposition numbers CCDC 2514802 (**L1**), 2514803 (**Si2b**), 2514804 (**Si3**, polymorph a), 2535198 (**Si3**, polymorph b), 2514805 (**Si4**; obtained from *n*-hexane) and 2535199 (**Si4**; obtained from *n*-pentane). The data can be obtained free of charge via https://www.ccdc.cam.ac.uk/structures/. The electronic energies of all optimised and calculated structures are summarised in the Supporting Information together with the corresponding references of the applied methods. The Cartesian coordinates of the structures are provided in the Supporting Data File. These files comprise all the necessary data for reproducing the values. The authors have cited additional references within the Supporting Information [111–132].

Supporting File 1: anie72143-sup-0001-SuppMat.pdf.

Supporting File 2: anie72143-sup-0002-Data.zip.